

Enhanced Water Management of High-Surface-Density Ni Foam as Flow Field for PEM Fuel Cells

Yuzhen Xia, Zichen Wang, Jiedong Wang, Lili Cao, Yousheng Xu and Guilin Hu*

School of Mechanical and Energy Engineering, Zhejiang University of Science & Technology, Hangzhou 310023, China

*E-mail: enehgl@163.com

Received: 2 November 2021 / Accepted: 13 December 2021 / Published: 5 January 2022

Ni foam with high surface density, has been proposed as an alternative flow field for PEM fuel cells, owing to large contact area, enhanced electron transport and low ohmic loss. The effect of pore diameter of Ni foam with high surface density above $1500 \text{ g}\cdot\text{m}^{-2}$ on physical parameters and cell performances was studied by polarization curves and EIS. Higher porosity, larger width of rib and higher flow field volume were obtained with pore diameter increasing. However, the cell performances of Ni foam were restricted, while larger R_{Ω} and R_{ct} was depicted because of lower internal surface area. The water management Ni foam with optimal pore diameter of $450 \mu\text{m}$ was studied at flood, moderate and dry state, respectively. As humidity temperature increasing from 20 to 50°C , the power density increased, even at extremely flooding state. High-surface-density Ni foam behaved excellent mass transfer properties for reactant gas and liquid water in water management of PEM fuel cells.

Keywords: Ni foam, Surface density, Pore diameter, Water management

1. INTRODUCTION

In fuel cells, bipolar plates (BPs) are used as multifunctional components in fuel cells, as current collectors and flow fields for reactants, accounting for above 80% of the weight and over 30% of the cost [1-3]. The study of BPs, aiming to improve fuel cell performance, reduce weight, and to save cost, is essential in low temperature proton exchange membrane (PEM) fuel cells development. The materials for BPs are required to behave high corrosion resistance, high mechanical strength, low ohmic resistance, light weight and low cost [4]. Despite low contact resistance and high stability, the application of graphite BPs is restricted because of the drawbacks including high cost and brittleness [5,6]. These problems have been aggravated by the complicated design of flow field, which affects the distribution and transfer of reactant gas, water management, fuel utilization, and ultimately the output of fuel cells

[7-10]. The studies in gas flow field contain designing novel channel flow and optimizing the structure of common flow fields, to obtain uniform distribution of current, low pressure drop, high mass transfer ability, therefore high cell performance and longer life. The opportunity is giving back to metal BPs, with easy processes ability and high strength, such as stainless steel and nickel alloys [11-13].

Metal foam, with good mechanical properties and light weight, has been broadly applied in renewable energy industry, for example, as the heat exchangers for solar energy collection systems to improve the heat transfer efficiency [13]. Metal foam used as the flow field for fuel cells, has attracted a lot of attentions, whose performances were compared with ordinary graphite serpentine flow field [14-18]. As the surface density increased, the contact area between gas diffusion layer (GDL) and flow field increased, resulting in enhanced electron transport and low ohmic loss. In addition, the porosity and pore size were optimized, for enough support strength and high contact area of the flow field [19].

Water management, which significantly affects catalyst and membrane degradation, is of vital importance for the life of PEMFC. Poor water management causes dehydration and flooding [20]. Ahrae Jo et al. [21] investigated the effects of using porous metal foam based BPs under practical automotive fuel cell operations with low humidification reaction gases. The water management capabilities of metal foam based BP designs were evaluated, compared to the traditional serpentine flow field BP designs. In both the experimental data and simulation results, the use of metal foam flow field mode resulted in less severe oxygen depletion, better membrane hydration and more uniform current density than using the serpentine flow field mode.

Ni foam has been widely used in new energy industry because of low price. Ni foam with high surface density, used as the flow field for PEM fuel cells, could ensure large contact area between flow field and GDL, enhanced electron transport and low ohmic loss. However, the effect of pore diameter and water management of high-surface-density Ni foam has been rare discussed. Ni foams with porosity above 95% and surface density above $1500 \text{ g}\cdot\text{m}^{-2}$, were studied in this work. The effect of pore size on the cell performances, the ohmic resistance and mass transfer properties were further discussed to optimize the foam structures. The mass transport abilities of metal foam flow field were then investigated at various humidity state.

2. EXPERIMENTAL

2.1 Fabrication of MEA

The catalyst ink containing Pt/C catalyst (20 wt.%, Shanghai Hesun Electric Co., Ltd), solvent (isopropanol/water) and Nafion dispersion (10wt.% in water, Dupont), was ultra-sonicated and then sprayed onto a micro-porous layer coated carbon paper (HCP120, Shanghai Hesun Electric Co., Ltd) with an airbrush. The Pt loading on the electrodes was around $0.2 \pm 0.02 \text{ mg}\cdot\text{cm}^{-2}$. An anode and a cathode were hot-pressed on the two sides of Nafion[®] membrane (Dupont NRE-212) at 135°C and 0.4 MPa, for 3 min to obtain a $3\times 3 \text{ cm}^2$ MEA.

2.2 Single cell system

Porous Ni foam (Kunshan Lvchuang Electronic Technology Co., Ltd), with a surface area of 9 cm^2 were placed into the groove of metal bipolar plate housing, used as flow field for anode and cathode, as shown in Figure 1(a). Ni foam pieces with porosity above 95%, surface density around $1500 \text{ g}\cdot\text{m}^{-2}$, but different pore size ($450 \mu\text{m}$, $580 \mu\text{m}$ and $800 \mu\text{m}$), were tested in PEM fuel cell.

A single cell, only containing heating element, composite bipolar plate with Ni foam, gaskets and MEA, was assembled. In the fuel cell test system, hydrogen and nitrogen from gas cylinders, was supplied to the anode through a pressure regulating valve and a gas flowmeter. Air was pressurized by an air compressor and passed through a pressure regulating valve, a humidifier and a gas flowmeter. Two heating pads on the anode and cathode, respectively, were used to control the fuel cell operating temperature.

2.3 Electrochemical tests

N_2 was supplied to the anode to purge the system at first, with a flow rate of $200 \text{ mL}\cdot\text{min}^{-1}$ for 10 min. Hydrogen and air were supplied to anode ($50 \text{ mL}\cdot\text{min}^{-1}$) and cathode ($120 \text{ mL}\cdot\text{min}^{-1}$), respectively. The temperature of humidifier was recorded as T_h , which was controlled by the water bath. The fuel cell temperature (T_c) was regulated by the heating elements.

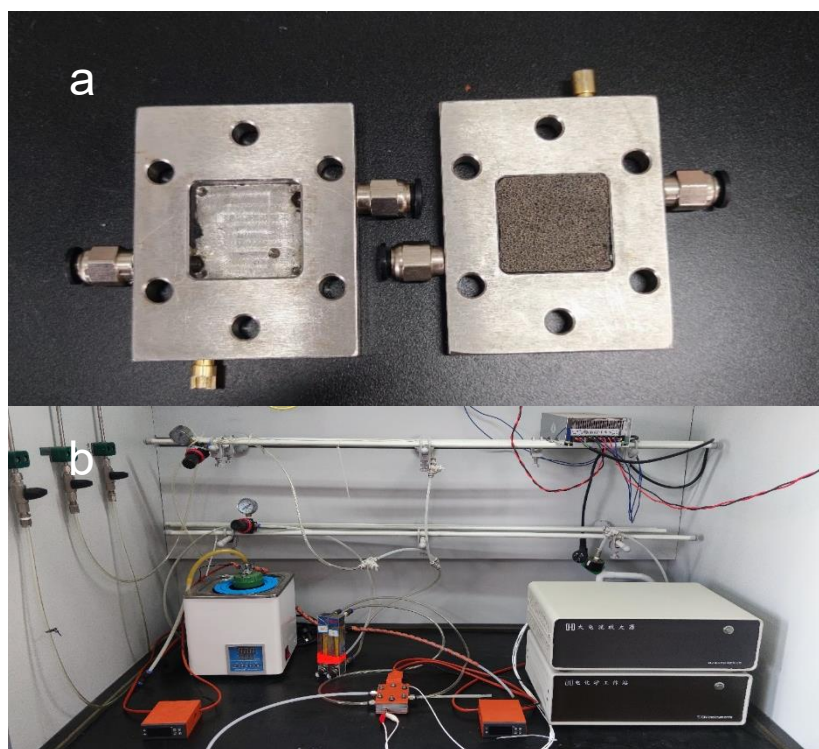


Figure 1. Photograph of bipolar plates embedded with Ni foam (a) and single fuel cell test system (b).

I-V curve was obtained by adjusting the potential variations, with a voltage limit of 0.25V. Electrochemical impedance spectroscopy (EIS) was employed on an electrochemical analyzer (CHI604E, Shanghai Chenhua Instrument Co., Ltd, China), to measure the resistances of the single cells. From 10 kHz to 50 MHz, the impedance measurements were performed at 0.8 V with 5 mV amplitude.

3. RESULTS AND DISCUSSION

The microphotograph of Ni metal foam with different pore size was shown in Fig. 2. The shape of the open cell was not fixed, mostly close to pentagon or hexagon. The average pore diameter for the three metal foam was around 450 μm, 580 μm and 800 μm, with the thickness of rib around 120 μm, 200 μm and 240 μm, respectively. The contact area per mm² GDL was estimated based on the suppose of hexagon cell and circle pore [22]. The physical parameters of metal foam were given in Table 1. As pore size increased, width of rib, porosity and path volume increased. The contact area between the Ni foam and GDL, was related to width of rib, surface density and pore size. All the three metal foam had contact area above 60% of the abstract surface area. Metal foam with a large number of metal ribs behaved a low intrinsic electrical conductivity and large contact area with GDL [23].

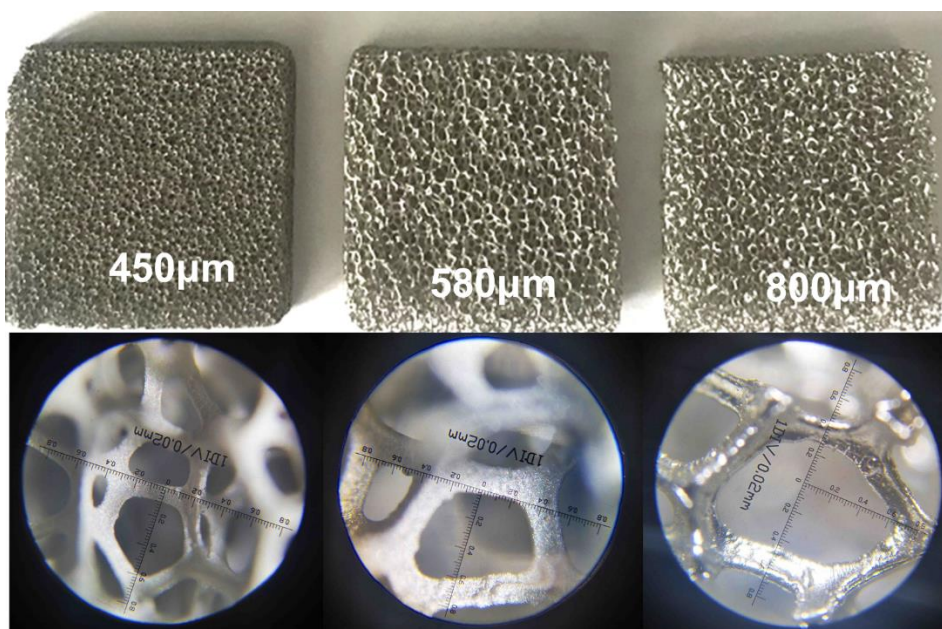


Figure 2. Microphotograph of Ni metal foam with pore size of 450 μm, 580 μm and 800 μm

Table 1. The physical parameters of Ni foam

Pore size / μm	450	580	800
Width of rib / μm	120	200	240
Contact area / cm²·cm⁻²	0.61	0.68	0.64
Porosity / %	95.4	95.7	96.7
Flow field volume / cm³	4.29	4.31	4.35

The effect of pore diameter in cell performances was studied and the polarization curves of the single cells with Ni foam flow fields of different pore diameter, were shown in Fig. 3, tested at $T_h = 20^\circ\text{C}$ and $T_c = 20^\circ\text{C}$. The working potential at $0.05 \text{ A}\cdot\text{cm}^{-2}$ decreased obviously as metal foam with larger pore was used. At minimum working voltage of 0.25 V, the maximum current density was 191 ($450 \mu\text{m}$), 107 ($580 \mu\text{m}$) and 83 ($800 \mu\text{m}$) $\text{mA}\cdot\text{cm}^{-2}$, respectively. The power density of Ni $800 \mu\text{m}$ was $23.1 \text{ mW}\cdot\text{cm}^{-2}$, only half of the value of $450 \mu\text{m}$ Ni, $49.3 \text{ mW}\cdot\text{cm}^{-2}$.

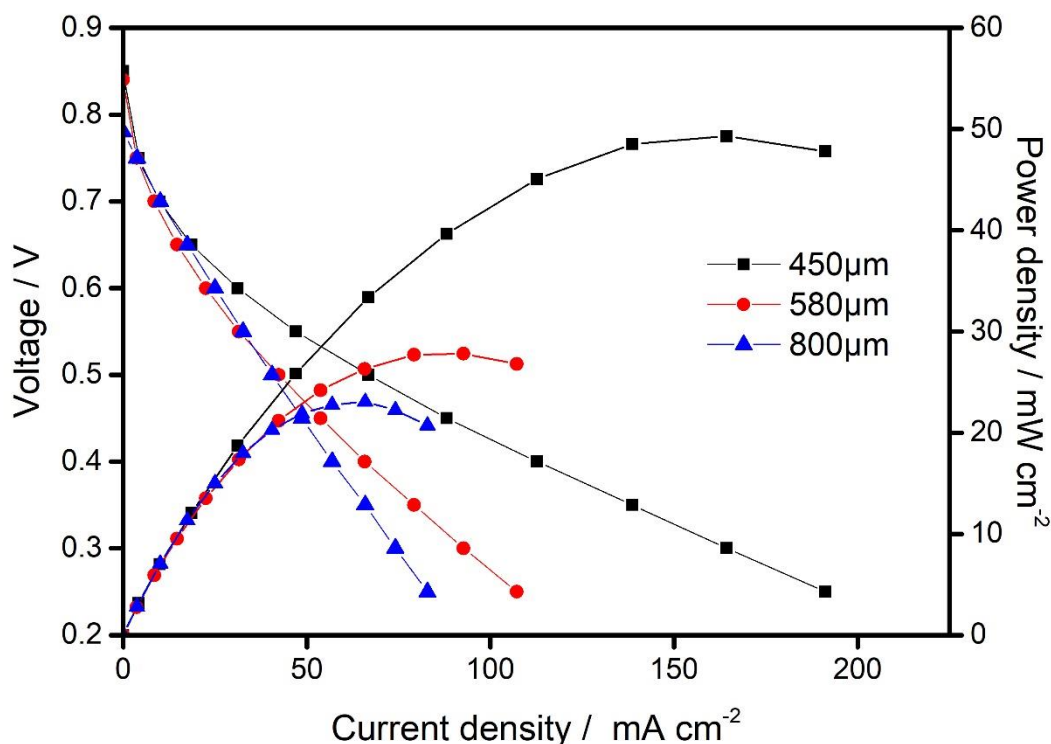


Figure 3. Effect of Ni foam pore size on fuel cell performances at $T_h = 20^\circ\text{C}$ and $T_c = 20^\circ\text{C}$

The intersection of the real axis measured at high frequency implies the total internal ohmic resistance of the cell including the contact resistance and ohmic resistance of cell components such as the bipolar plate, GDL, membrane and catalyst layer [24]. The pore sizes and structures in metal foam flow field resulted in different ohmic losses. For metal foams with large pore sizes, may result in larger ohmic losses [25]. As shown in Table 2, its value, equal to the diameter of the Nyquist plots, was 0.042, 0.073 and $0.11 \Omega\cdot\text{cm}^{-2}$, respectively. Higher pore size also resulted the charge transfer route increasing during the electrochemical reaction. Therefore, larger R_Ω and R_{ct} , depicted in the impedance investigation while Ni foam with large pore was used as the flow field, was consistent with the results shown in polarization curves. The cell performance decreased with increasing pore size was due to increased charge-transfer resistance caused by reduced internal pressure and mass transport resistance. As the pore size of the foam was large, the internal surface area was reduced, which led to a decrease in the form drag, thereby reducing pressure change [26].

Since the proton conductivity of the membrane is strongly dependent on the water content in it, the performance of the fuel cell is highly relied on external humidification. But the actual working humidity status of the membrane is difficult to monitor. In this work, we evaluated the working humidity of the membrane with the relative humidity of the outlet gas.

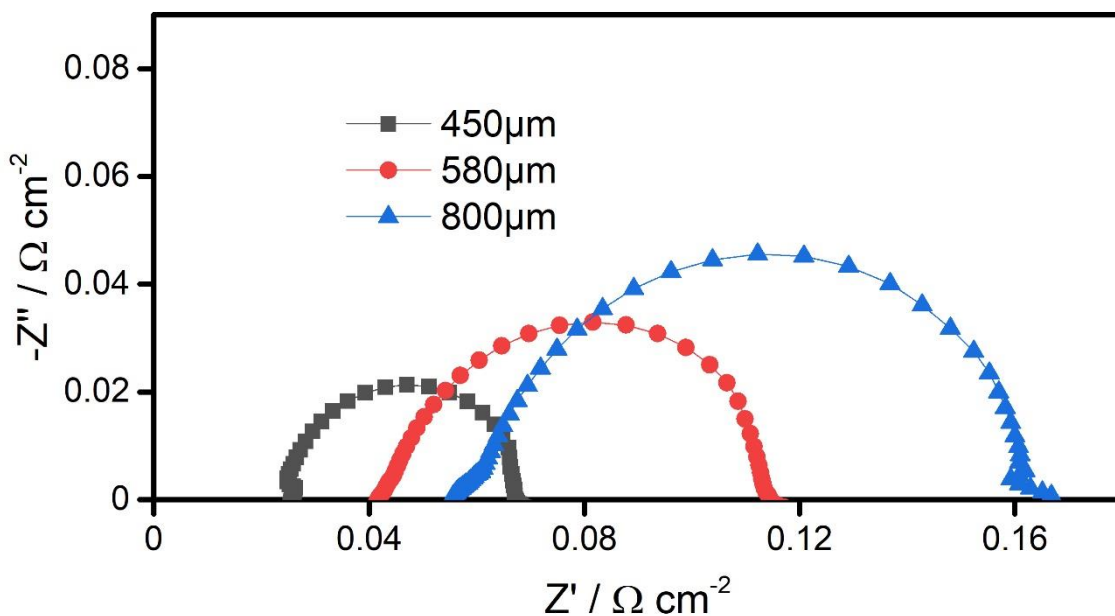


Figure 4. Nyquist plots of single cells with Ni foam flow field of different pore size at $T_h = 20^\circ\text{C}$ and $T_c = 20^\circ\text{C}$

Table 2. The EIS parameters of single cells with Ni foam flow field of different pore size at $T_h = 20^\circ\text{C}$ and $T_c = 20^\circ\text{C}$

Pore size / μm	450	580	800
$R_\Omega / \Omega \cdot \text{cm}^{-2}$	0.025	0.042	0.055
$R_{ct} / \Omega \cdot \text{cm}^{-2}$	0.042	0.073	0.11

Table 3. Relative humidity (%) of outlet gas under various working temperature and humidity temperature

T_c ($^\circ\text{C}$) \ / \ T_h ($^\circ\text{C}$)	20	40	50
20	392	487	581
30	216	269	320
40	124	154	184
50	74	92	110

Assumed that the inlet air in cathode has been well humidified, the relative humidity of outlet gas [27]:

$$\Phi = \frac{(0.420 + \varphi\lambda)P_{out}}{(1 + \varphi)\lambda + 0.210} \cdot \frac{1}{P_{sat}}$$

, where λ is the stoichiometric ration of air, $\lambda=5$; P_{out} is the overall pressure of outlet gas, $P_{out} = 1$ atm; P_{sat} is the saturation vapor pressure of water at T_c ; φ is the proportion of water vapor in the inlet air. The obtained relative humidity of outlet at various T_h and T_c has been given in Table 3.

The outlet gas contained redundant oxygen, nitrogen and water from humidification and reaction product. Based on the assumption that all water in vapor was brought out by exit air with no water migration from cathode to anode and no fluid retention in flow field or electrodes, the estimated outlet relative humidity could partially reflect the humidity state in the fuel cell. In many researches, the fuel cell relative humidity was estimated as 100% when T_h was equal to T_c . However, the actual relative humidity of the exit gas varied from 392% to 110% with cell temperature from 20°C to 50°C. Therefore, the relative humidity of outlet at various T_h and T_c was more reliable to characterize the operating humidity conditions of fuel cells.

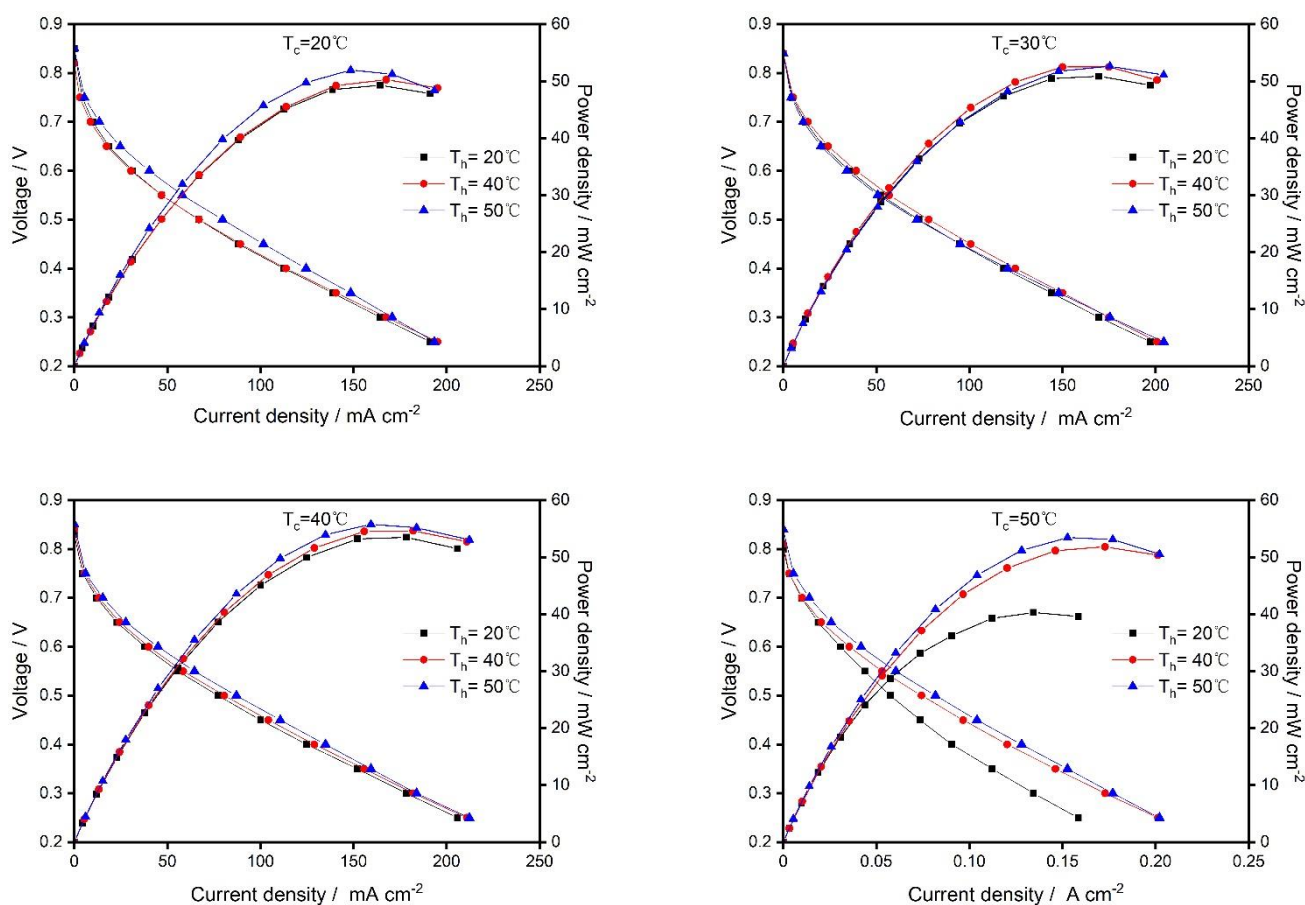


Figure 5. Polarization curves of fuel cell with Ni foam (450 μm) flow field at $T_c = 20/ 30/ 40/ 50^\circ\text{C}$; $T_h = 20/ 40/ 50^\circ\text{C}$

As T_h increasing, more water vapor in cathodic air was brought into the system, and therefore the

relative humidity of outlet gas increased. The water vapor easily converted to liquid which was trapped in the flow field at low T_c , corresponding to the high relative humidity above 100%. The value decreased as T_c increases from 20°C to 50°C, as the humidify state switched in flood state (20 and 30°C), moderate state (40°C), and dry state (50°C), respectively.

The performances of fuel cell with 450 μm Ni foam as flow field was tested at various humidity condition. Their polarization curves at different T_h and T_c were studied, as shown in Fig. 5. At $T_c = 20^\circ\text{C}$ with high relative humidity above 392%, the power density increased with T_c , although slight decrease was observed at high current density. The 3-D porous structure offers high flow field volume for reactant and therefore enhanced the mass transfer ability in extremely flood state [27]. Meanwhile, as warm reactant was bought into the cathode at high T_h , the fuel cell performances was improved. The same phenomena appeared at moderate state (40°C) and dry state (50°C). The fuel cell performance was first enhanced as T_c increased because of high i_0 . The peak power density, 54.9 $\text{mW}\cdot\text{cm}^{-2}$, was observed at $T_c = 40^\circ\text{C}$. As T_c increased up to 50°C, dry membrane may restrict the proton transfer in the electrochemical reaction and resulted the decline in cell performances.

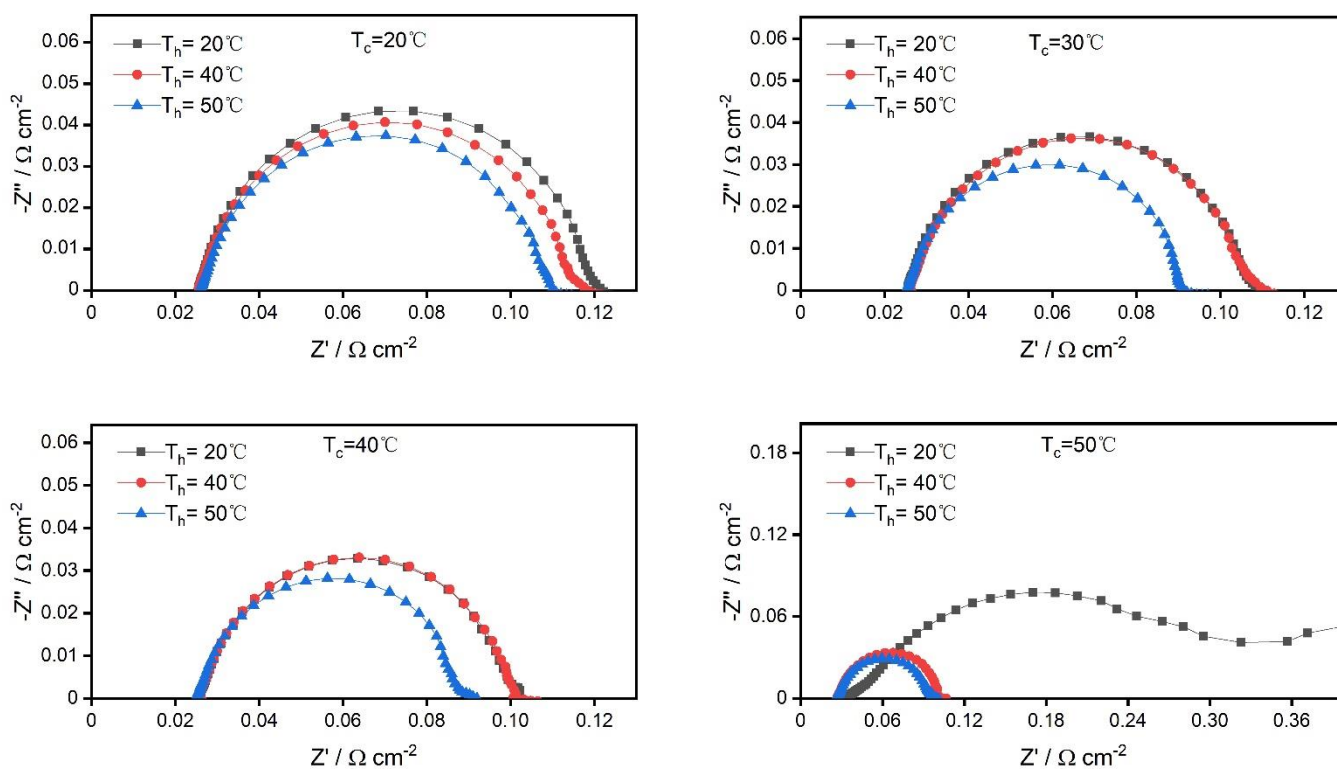


Figure 6. Nyquist plots of single cell with Ni foam (450 μm) flow field at $T_c= 20/ 30/ 40/ 50^\circ\text{C}$; $T_h= 20/ 40/ 50^\circ\text{C}$

The effect of working condition was then investigated in EIS. In Figure 6, the Nyquist plots tested at 0.8V showed only one loop. As shown in Table 4, the intersection value at Z' axis, equal to R_Ω , was around 0.025 $\Omega\cdot\text{cm}^{-2}$ at flood and moderate state. The value increased nearly 85% at extremely dry

state, $0.032 \Omega \cdot \text{cm}^{-2}$, $T_c = 50^\circ\text{C}$ and $T_h = 20^\circ\text{C}$. The charge transfer resistance R_{ct} , $0.096 \Omega \cdot \text{cm}^{-2}$, was determined by the diameter of the impedance loop. At $T_c = 20^\circ\text{C}$, the diameter of the impedance loop gradually decreased as the humidification temperature reached to 50°C , showing a better resistance to flooding. Its value decreased as T_c increased to 40°C , indicating lower activation polarization at higher temperature, which was corresponded with the conclusions in polarization curves. When relatively low external humidification was applied ($T_h = 20^\circ\text{C}$) and in the same time cell temperature was maintained high ($T_c = 50^\circ\text{C}$), an increase in proton transport resistance was expected due to the fact that membrane became less hydrated and its proton conductivity got low [23].

Table 4. The values of R_Ω ($\Omega \cdot \text{cm}^{-2}$) and R_{ct} ($\Omega \cdot \text{cm}^{-2}$) in single cell with Ni foam ($450 \mu\text{m}$) flow field at $T_c = 20/ 30/ 40/ 50^\circ\text{C}$; $T_h = 20/ 40/ 50^\circ\text{C}$

$T_h / ^\circ\text{C}$	$T_c / ^\circ\text{C}$							
	20		30		40		50	
	R_Ω	R_{ct}	R_Ω	R_{ct}	R_Ω	R_{ct}	R_Ω	R_{ct}
20	0.025	0.096	0.026	0.084	0.026	0.084	0.032	0.34
40	0.026	0.093	0.026	0.085	0.026	0.085	0.027	0.077
50	0.026	0.083	0.026	0.066	0.026	0.066	0.027	0.072

4. CONCLUSIONS

Ni foam with high surface density above $1500 \text{ g} \cdot \text{m}^{-2}$ was assembled into a single cell for testing, and the effect of pore diameter on cell performances was discussed. Higher surface density resulted high contact area between gas diffusion layer and flow field, above 60% of surface area. Although higher porosity, larger width of rib and higher flow field volume were presented as pore diameter increased, the cell performances declined because of lower internal surface area. Larger R_Ω and R_{ct} was depicted while Ni foam with larger pore diameter of $580 \mu\text{m}$ and $800 \mu\text{m}$ was tested. Ni foam with pore diameter of $450 \mu\text{m}$ was proved to be the optimal flow field for PEM fuel cell, because of high electron and charge conductivity, which also exhibited high anti-flood performance. The power density increased as cell temperature and humidity temperature, which could be attributed to the excellent mass transfer properties of Ni foam even at extremely flooding state. High-Surface-density Ni foam, with 3-D porous structure could offer a large number of gas and liquid path and shows enormous potential in water management.

ACKNOWLEDGEMENTS

We gratefully acknowledge the support from National Nature Science Foundation of China (No. 11972324) and from Department of Education of Zhejiang Province (No. Y201839674).

References

1. H. Tawfik, Y. Hung and D. Mahajan, *J. Power Sources*, 163 (2007) 755-767.

2. R. Taherian, *J. Power Sources*, 265 (2014) 370-390.
3. Y. Song, C. Zhang, C.Y. Ling, M. Han, R.Y. Yong, D. Sun and J.R. Chen, *Int. J. Hydrogen Energy*, 45 (2019) 29832-29847.
4. D. Qiu, L. Peng, P. Yi, X. Lai and W. Lehnert, *Energy Convers. Manage.*, 174 (2018) 814-823.
5. P. Liang, D. Qiu, L. Peng, P. Yi, X. Lai and J. Ni, *Energy Convers. Manage.*, 169 (2018) 334-344.
6. B.H. Lim, E.H. Majlan, W.R.W. Daud, T. Husaini and M.I. Rosli, *Ionics*, 22 (2016) 301-316.
7. J. Shen, Z. Tu and S.H. Chan, *Energy Convers. Manage.*, 213 (2020) 112841.
8. H. Guo, M.H. Wang, J.X. Liu, Z.H. Nie, F. Ye and C.F. Ma, *J. Power Sources*, 273 (2015) 775-783.
9. H. Heidary, M.J. Kermani and B. Dabir, *Energy Convers. Manage.*, 124 (2016) 51-60.
10. P. Alnegren, J.G. Grolig, J. Ekberg, G. Göransson and J.E. Svensson, *Fuel Cells*, 16 (2016) 39-45.
11. N.F. Asri, T. Husaini, A.B. Sulong, E.H. Majlan and W.R.W. Daud, *Int. J. Hydrogen Energy*, 42 (2017) 9135-9148.
12. S.Y. Tsai, C.H. Lin, Y.J. Jian, K.H. Hou and M.D. Ger, *Surf. Coat. Technol.*, 313 (2017) 151-157.
13. M. Kim, C. Kim and Y. Sohn, *Fuel Cells*, 18 (2018)123-128.
14. C.Y. Ahn, M.S. Lim, W. Hwang, S. Kim, J.E. Park, J. Lim, I. Choi, Y.H. Cho and Y.E. Sung, *Fuel Cells*, 17 (2017) 652-661.
15. S. Huo, N.J. Cooper, T.L. Smith, J.W. Park and K. Jiao, *Appl. Energy*, 203 (2017) 101-114
16. C.J. Tseng, Y.J. Heush, C.J. Chiang, Y.H. Lee and K.R. Lee, *Int. J. Hydrogen Energy*, 41 (2016) 16196-204.
17. W.C. Tan, L.H. Saw, H. San Thiam, J. Xuan, Z. Cai and M.C. Yew, *Renewable Sustainable Energy Rev.*, 96 (2018) 181-197.
18. B.T. Tsai, C.J. Tseng, Z.S. Liu, C.H. Wang, C.I. Lee, C.C. Yang and S.K. Lo, *Int. J. Hydrogen Energy*, 37 (2012) 13060-13066.
19. X. Yang, J. Yu, Z. Guo, L. Jin and Y.L. He, *Appl. Energy*, 239 (2019) 142-156.
20. P. Pei and H. Chen, *Appl. Energy*, 125 (2014) 60-75.
21. A. Jo and H. Ju, *Int. J. Hydrogen Energy*, 43 (2018) 14012-14026.
22. D.K. Shin, J.H. Yoo, D.G. Kang and M.S. Kim, *Renewable Energy*, 115 (2018) 663-675.
23. C.J. Tseng, B.T. Tsai, Z.S. Liu, T.C. Cheng, W.C. Chang and S.K. Lo. *Energy Convers. and Manage.*, 62 (2012) 14-21.
24. H. Lee, H. Kim and H. Kim, *J. Electrochem. Soc.*, 166 (2019) 74-78.
25. G. Zhang, Z. Bao, B. Xie, Y. Wang, K. Jiao, *Int. J. Hydrogen Energy*, 46 (2021) 2978-2989.
26. J.E. Park, W. Hwang, M.S. Lim, S. Kim, C.Y. Ahn, O.H. Kim and Y.E. Sung, *Int. J. Hydrogen Energy*, 44 (2019) 22074-22084.
27. Y. Xia, H. Zhu, Z. Wang, F. Sun, Y. Xu and G. Hu, *Int. J. Electrochem. Sci.*, 16 (2021) 1-5.